2015 IEEE/RSJ International Conference on Intelligent Robots and Systems (IROS)
Congress Center Hamburg
Sept 28 - Oct 2, 2015. Hamburg, Germany

Hydrodynamic function of a robotic fish caudal fin: effect of kinematics and flow speed

Ren Ziyu, Wang Tianmiao, Wen Li *Member, IEEE*

***Abstract*—Fish caudal fin is a prominent example of biological propulsion, in which the caudal peduncle, fin rays and fin membrane together form a dynamic locomotory system. In this paper, we developed a bio-robotic model to mimic the caudal fin structure and kinematics of Bluegill Sunfish (*Lepomis macrochirus*). We coupled controlled oscillations in both heave and pitch directions to the robot to model the caudal peduncle motion of swimming fishes. Synchronized multi-axis force transducer and particle image velocimetry were then used to quantify the hydrodynamic forces and wake flow in the vertical plane. We found that changing the flow speed and the phase *b*etween the caudal fin ray and peduncle locomotion resulted in significantly different lift and thrust force. DPIV results showed that the vortex jet angle changed with flow speed and phase φ. According to current experiment, we hypothesized that the fish caudal fin may function as a "flexible vectoring propeller", and may be responsible for the three-dimensional maneuverability of fishes.**

I. Introduction

The analysis of non-traditional biomimetic propulsion under controlled conditions has attracted mathematicians [1], fluid engineers [2], roboticists [3-5], material engineers [6]and biologists' [7, 8]interests in studying the principles underlying unsteady locomotion in aquatic animals. Fish caudal fin is a prominent example of biological propulsion, in which the caudal peduncle, fin rays and fin membrane together form a dynamic locomotory system. Caudal fin of most bony fishes, which occupies 88% of entire fresh & salt water fish species, move in complex three-dimensions, and move harmonically with caudal peduncle for different swimming behaviors, such as prey, escape and long-time migration [9-11].

Bony fishes can actively control both caudal peduncle muscle and deform the caudal fin surface through individually controlling the fin ray muscles. The peduncle motion is derived from the undulatory body wave generated by myotomal body musculature. While the fin rays are moved by a group of intrinsic musculatures (*interradialis and hypochordal longitudinalis*) that enable fin surface to form a variety of shapes [10]. Most previous biomimetic robotic propulsors focused on the thrust performance of two-dimensional flapping locomotion which contains heave & pitch movements that mimic the caudal peduncle motion [2, 12-14]. There are very few papers investigated the effect of flexure stiffness of fin rays, or the fin locomotor functions [15-19]. How do the caudal fin rays and peduncle function together on the hydrodynamics of propulsion remains completely unexplored.

How do the kinematics of the peduncle and the fin rays together determine the locomotor performance of a caudal fin? Can we use a robotic experimental device to mimic both the caudal peduncle and fin ray motions and is there an optimal phase relationship between these two? Does the homocercal tail during swimming generates wake flow and vortex jet angle that can boost fish horizontally or vertically, or both? And how does the swimming speed affect the locomotor forces generated by the caudal fin? To our knowledge, no experimental studies have yet addressed above issues, nor does any existing experimental hydrodynamic system could allow above questions to be investigated.

In this paper, we first designed and fabricated a robot to mimic the homocercal caudal fin of Bluegill Sunfish (*Lepomis macrochirus*), and programmed it with motions according to the biological data from previous studies [10, 20]. A heave and pitch robotic system was then implemented on the towing system, which allows coupling the fish caudal peduncle motion to the fin motions and move the robot in axial direction under controlled speeds. Then we simultaneously measured hydrodynamic forces and wake flow of the robot with different phase angles and at different flow speeds (0, 5 and 10 cm/s). Wake morphology measurements were conducted in the vertical (mid-sagittal, *xz*) plane (see Fig. 1 and 2 for notation) by DPIV method (digital particle image velocimetry). Finally, we discussed the biological relevance of current experimental results and formulate several suggestions for the developments of fish bio-robotics.

II. Materials And Methods

A. Bio-robotic Caudal Fin

The design of the robotic caudal fin was based on the anatomy of the Bluegill Sunfish [10, 15, 21]. Fig. 1(a) shows a schematic diagram of the robot. We used five fin rays to actuate the robotic caudal fin to mimic the fin membrane deformation of its biological counterpart. Each fin ray was individually actuated by a servo motor (MG995, HuiSheng Inc., China) which was controlled by the PWM (pulse-width-modulation) signal output from the microcontroller (STM32, STMicroelectronics Inc., EU) for controlling the angular position. All five servo motors pulled nylon tendons (with diameter of 0.6mm) that were attached to both sides of each fin base and drove the fin rays to move side-to-side (indicated in Fig. 1(a) with solid yellow arrow).

This work was supported by the National Science Foundation support projects, China under contract number 61403012, Beijing Science Foundation support projects under contract number 4154077 and National Science Foundation support projects, China under contract number 61333016. Authors are with the School of Mechanical Engineering and Automation, Beihang University, Beijing, 100191, People's Republic of China; e-mail for contact: liwen@buaa.edu.cn).

The fin membrane was fully expanded by elastic bungees. This design also allowed the caudal fin to have a passive compliance in the folding direction (indicated in Fig. 1(a) with dashed red arrow). The snapshot of the robotic caudal fin was shown in Fig. 1(b).The size of the fully expanded membrane was 170 mm in chordwise length and 90 mm in spanwise length. The bony components such as fin rays and streamlined shells were all fabricated with PLA (polylactic acid) by using a 3D printer (Makerbot replicator2, MakerBot Inc., NY, USA). Two layers of silicone membranes with thickness of 300 μm were pasted on both sides of fin rays. More details of the mechanical design can also be found in our previous work [22].

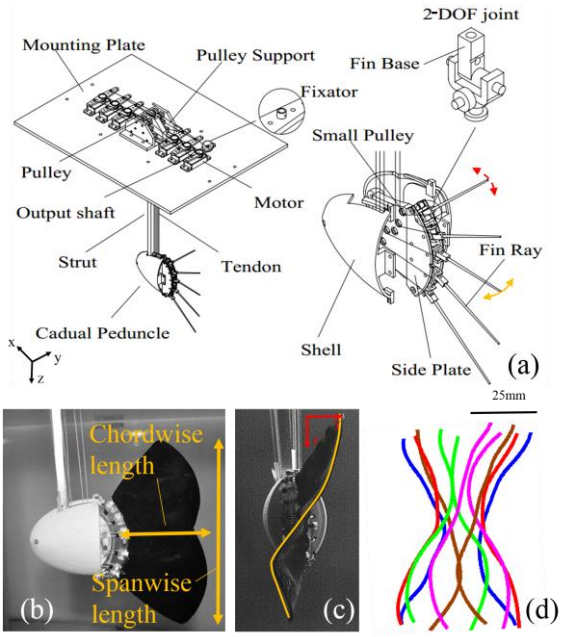

Figure 1. (a) Robotic caudal fin demonstration in Solidworks (Solidworks 2013, Dassault Systemes Inc., FRA). The tendons were fixed with output shaft using a fixator, then wrap around low-friction idle pulleys and eventually fixed to both side of the fin base. Fixators mounted on the output shaft can be used to adjust the preload of the nylon tendons. A streamline-shape shell was used to cover the caudal peduncle. The swing and fold movements were illustrated with solid yellow and dashed red arrows respectively. (b) The snapshot of the robotic model. We used black silicone rubber for fin membrane in order to minimize the reflection of the laser, therefore to obtain better high speed camera DPIV images. (c) Snapshot of the kinetic caudal fin at one time instant from the rear, the yellow curve indicates the trailing edge of the caudal fin; (d) Curves of trailing edge digitized from high speed images during a complete flapping cycle at U=0 cm/s, φ=0°.

B. Kinematics modeling

The undulatory wavy locomotion along the dorsal-ventral direction was most commonly observed during swimming of bony fishes [15]. To model caudal peduncle motion and fin ray motion, a reference frame was settled on a transverse plane with the origin having a same ordinate value with the uppermost fin ray tip as shown in Fig. 1(c). The mathematical model of the undulation motion of the caudal fin can be expressed as follows:

$$y(z,t)=a_u\sin(2\pi ft-2\pi z/\lambda+\varphi) \quad (1)$$

where y is the horizontal displacement of the fin ray tip with ordinate of z at the time t relative to the moving caudal peduncle. a_u indicates the amplitude, f is the motion frequency and λ is the undulation wavelength. φ is the phase angle between caudal peduncle motion and caudal fin ray motion. For all experimental trials, the amplitude a_u, the frequency f and the wavelength λ were fixed to 20 mm, 1 Hz and 170 mm, respectively. The rotation angle of the fin base can be derived from:

$$\vartheta_i(t)=\arcsin(y_i(t)/r_i) \quad (2)$$

where ϑ_i is the rotation angel of the ith fin base, and r_i is the length of the ith fin ray. y_i denotes the horizontal displacement of the ith fin ray which is derived from (1). The caudal peduncle motion of live fish can be resolved into heave and pitch motions and can be expressed as follows:

$$y_h(t)=h\sin(2\pi ft) \quad (3)$$

$$y_p(t)=p\sin(2\pi ft+90°) \quad (4)$$

where y_h denotes the caudal peduncle displacement on horizontal plane and y_p denotes the rotated angel around axis z. h indicates the heave amplitude and p indicates the pitch amplitude. To make the robotic caudal fin move like a vivo fish, the value of h and p were set as 10 mm and 8° respectively. A camera was set right behind the caudal fin to record the high speed images of the fin membrane trailing edge. Fig. 1(c) shows a snapshot of the robotic fin undulation motion coupling with heave and pitch motions (at φ=0°, U=0 cm/s) at one flapping instant. Fig. 1(d) shows the trailing edge trajectories during a whole flapping cycle digitized from the high speed camera images.

C. Hydrodynamic characterization

Fig. 2(a) shows the schematic view of the experimental apparatus for the hydrodynamic characterization. The water tank had a dimension of 7.8 m in length, 1.2 m in width and 1.1m in height. A guide rail that was actuated by a 4000 watt AC motor with a travel distance of 7.5 m, a position accuracy of 0.1 mm and a maximum speed of 3 m/s was set vertically above the water tank, and was used to generate precisely controlled towing speed (U, indicated in Fig. 2(a)). A carriage assembled with the guide rail integrated capabilities of both translational and rotational movements. The translational (heave) and rotational (pitch) motions were actuated by servomotors and were used for generating heave and pitch motions of the caudal peduncle (illustrated in Fig. 2(a)). For all experiments, the robotic caudal fin moved at mid-depth of the water tank to minimize the interference effect of the free surface and the bottom of the tank. More details of the towing system and water tank can also be found in our previous works [4, 5, 23].

To measure the hydrodynamic forces generated by the robotic caudal fin, a multi-axis force transducer (mini-40, ATI Industrial Inc., Canada) was mounted between the heave & pitch plate and the bio-robotic caudal fin model (Fig. 2(a)). The force transducer allows three forces, i.e. forces in x, y and z directions, to be measured simultaneously. The force data were collected by a DAQ card (PCI-6284, National Instrument

Inc., USA). Two-dimensional digital particle image velocimetry (DPIV) was used to obtain a qualitative and quantitative description of the flow patterns generated by the moving robotic caudal fin. The wake flow was visualized by seeding the water with near-neutrally buoyant glass beads that is 20 μm in diameter. The laser came from a 5 W laser with wavelength of 532 nm (MGL-N-532, Changchun Xinchanye Inc., Changchun, China). The laser beam was focused into a 1mm thick laser sheet and then projected vertically into the water on vertical (mid-sagittal) plane using an optic glass. A mirror with length of 3 m was placed at 45° to the horizontal plane at the bottom of the water tank. A high speed camera was used to record the particle images that reflected from the mirror with sample rate of 250 Hz. Fig. 2(b) shows a high speed camera image of the illuminated particles. The movement of the bio-robotic caudal fin, the acquisition of the force data and the high speed camera were all triggered by a signal from a Labview program (National Instrument Inc., USA).

High speed images with time duration of 10s were recorded during each trial, while the images of initial three seconds were removed from the image sequence in order to guarantee all the wake flow analyzed were in steady state. We then used a commercial software (LiFangTianDi Inc., Beijing, China) to obtain velocity and vorticity fields of the wake flow from these raw photos. The interrogation window we used was 32 pixels× 32 pixels (which is 4.2 mm×4.2 mm), and the overlapped between two consecutive windows was 50%. The velocity fields from 5 flapping cycles at the same instant were abstracted to obtain a phase-averaged velocity field result. This average velocity field result was then used to calculate vorticity field in Tecplot (Tecplot Inc., USA). To get the scale relation between the pixel and the actual length, we put a ruler right on the plane of the laser sheet. The scale was then obtained by reading the pixel length of the ruler on the screen.

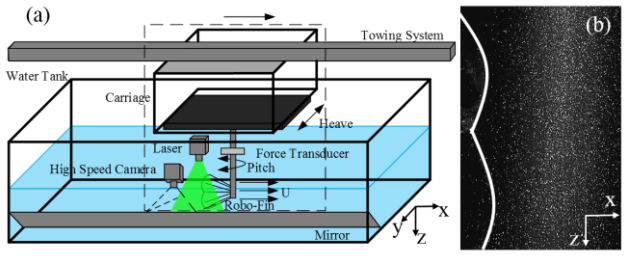

Figure 2. (a) Schematic view of the experimental apparatus; (b) High speed camera image of the illuminated particles in sagittal view. The white curve indicates the boundary of the trailing edge.

We used the vortex ring model [24] to estimate the wake vorticity generated by the robotic caudal fin . Illuminating the cross section through such a vortex ring should yield a flow pattern consisting of two vorticities with opposite rotational senses with a flow jet separating them apart. Definition of parameters of a vortex ring are shown in Fig. 3. For the purpose of simplifying the definition, we set up two coordinate systems on the vertical plane. The origin of the global coordinate system (NE) was based on the caudal fin notch and the E axes was parallel to the horizontal plane. The body coordinate system (N'E') was based on the vertical cross section of the vortex ring and the E' axes traveled through the centers of two vortexes.

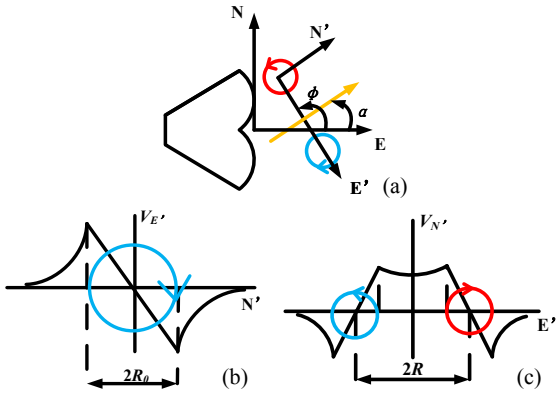

Figure 3. (a) Coordinate system and notation used to describe the vorticity of the caudal fin. The yellow arrow indicates the jet flow. (b) Definition of the vortex core radius R_0. (c) Definition of vortex ring radius R.

According to Milne-Thomson and Louis Melville's theory [24], the impulse I of a single vortex ring can be derived from:

$$I=\rho\Gamma\pi R^2$$

where I is the impulse we estimated from the shedding vortex ring. ρ is the density of the water and R is the vortex ring radius. Γ is the circulation of a vortex, namely, the line integral about a curve C enclosing the vortex. Γ can be derived from the following equation:

$$\Gamma=\oint_c v_t dx \qquad (6)$$

where dx is the differential element along curve C and v_t is the tangential velocity component about the curve C. Note that the jet flow vector and the line through the vortex centers (i.e. the E' axes) may be out of plumb actually. Following Milne-Thomson and Louis Melville [24], we calculated vortex core radius R_0 and vortex ring radius R by plotting the profiles of the velocity components V_N and V_E parallel to N' and E' respectively (see Fig. 3(b) and (c)).

III. Results

A. Hydrodynamic Force

We examined the mean thrust force and mean lift force (which were averaged from one flapping cycle) generated by undulation movement pattern under different towing speeds (U). The results show that the towing speed had great impact on the forces. From Fig. 4, it can be observed that when phase angle is zero (φ=0°), the mean thrust force decreased with increased flow speed. This may due to the fact that the drag force increased while towing speed increased. At U=0 cm/s, the maximum mean thrust force was 0.049 N. At U=5 cm/s and U=10 cm/s, the mean thrust force was -0.030 N and -0.064 N respectively, which is significantly smaller than that at U=0 cm/s. The lift force also decreased as the towing speed increased (Fig. 4(b)). At U=0 cm/s, the lift force was 0.074 N, which was significantly larger than that of U=5 cm/s and U=10 cm/s (0.029 N and 0.027 N, respectively). Overall, it can

be summarized that when the flow speed increased, the effect of three-dimensional fin ray locomotion became less significant; less hydrodynamic force will be obtained under high swimming speed than under low locomotion velocity.

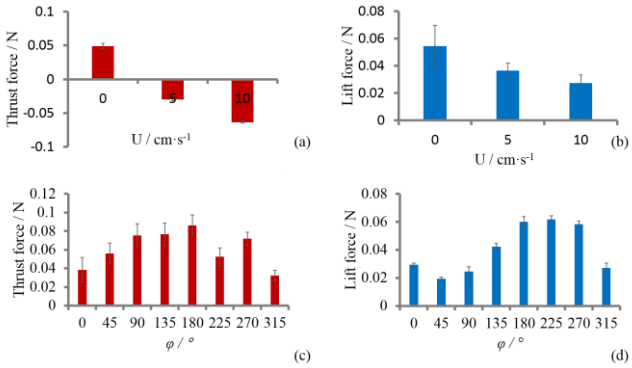

Figure 4. Mean thrust force (a) and lift force (b) under U= 0, 5 and 10 cm/s for undulation pattern were shown. (c)(d)Thrust force and lift force as function of phase angle (φ =0°~315°) between caudal peduncle and fin ray motion were tested under U=0 cm/s.

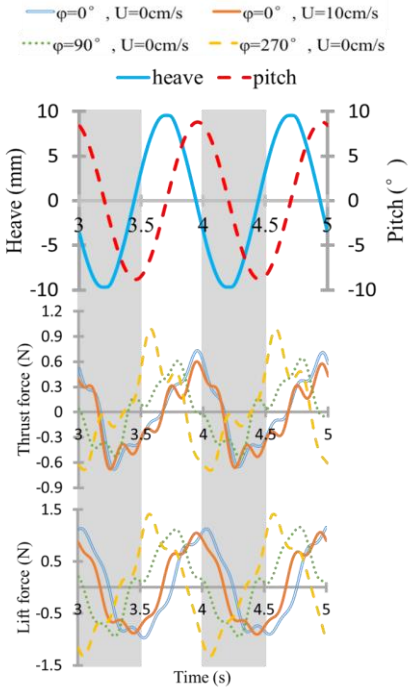

Figure 5. Heave and pitch motions (a) for two flapping cycles. Instantaneous thrust force (b) and lift force (c) for two flapping cycles under four selected movement patterns.

Experiments on thrust and lift force at different phase angles (φ) were then conducted. Mean thrust force and mean lift force varied significantly with φ (Fig. 4(c) and (d)). When φ=45°, mean thrust force reached its minimum value with magnitude of 0.030 N. When φ=225°, mean thrust force reached its maximal value with magnitude of 0.062 N. The peak-to-valley ratio was about 2.067. For mean lift force, peak value appeared at φ=180° which was 0.086 N. Valley value appeared at φ=315°which was 0.032 N. The peak-to-valley ratio was about 2.688. These data clearly demonstrate that the peduncle motion do have a significant impact on the hydrodynamic force of the robotic caudal fin.

Instantaneous force of different movement patterns during two flapping cycles (from 3s to 5s) were demonstrated in Fig. 5 with different colored curves. The force profiles of instantaneous thrust and lift force changed with increased flow speed (see red and blue curves in Fig. 5): the peaks and valleys appeared at the same time (i.e., at time T), however, the peak value at U=0cm/s was larger than that at U=10 cm/s. As φ changes, the force profiles shifted along time axis and differed in force magnitude (see green and yellow curve at time 0.75T and 0.5T): at φ=270°, the instantaneous force can obtain higher force magnitudes.

B. Wake Flow

We performed two-dimensional digital particle velocimetry under four kinematic conditions where interesting force results were found: 1) undulation motion at φ=0°, U=0 cm/s; 2) undulation motion at φ=0°, U=10 cm/s; 3) undulation motion at φ=90°, U=0 cm/s and 4) undulation motion at φ=270°, U=0 cm/s. Instantaneous wake flow are shown in Fig. 6 ~ 9. Moreover, the wake morphology parameters of vortex ring 1 ~ 7 are listed in Table I.

At φ=0°, U=0 cm/s, two vortex rings were shed from the middle part of the caudal fin during one flapping cycle at 0.8T and T (vortex ring no. 1 and 2, Fig. 6). Compared with vortex no. 1, vortex no. 2 had a smaller vortex core radius (R_0) and vortex ring radius (R) with significantly greater jet flow angle (α) but less vorticity circulation (Γ) and impulse (I). This indicates that the vortex no. 2 contained less energy, however, generated more lift force than vortex no.1. We therefore can conclude that lift force at φ=0°, U=0 cm/s mainly came from the impulse of vortex ring no. 2. When U=10 cm/s, the morphology of the vortex ring changed obviously (vortex no. 3 and 4, Fig. 7). The time instants of forming the vortex rings were in advance to 0.4T and 0.8T. The magnitude of R_0 of vortex no. 3 and 4 decreased by 52.7% and 50.6% than that of vortex no. 1 and 2, but R increased by 57.6% and 96.5%. Although the impulse of vortex ring no. 3 and 4 were enhanced significantly, the magnitude of α decreased significantly, which made the lift component of force decreased eventually. Besides, vortex ring no. 3 and 4 have opposite directions of jet angle (the values were opposite in sign, i.e.) and the lift impulse generated by these two vortex rings were therefore counterbalanced for an entire flapping cycle.

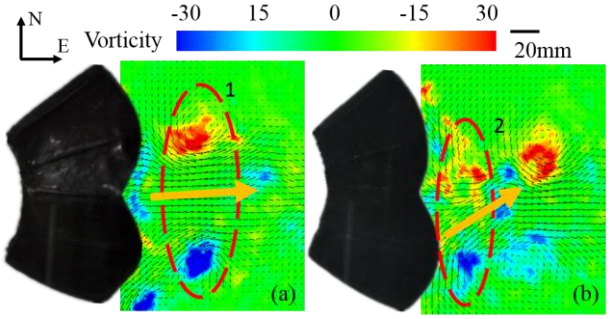

Figure 6. Instantaneous wake flow under U=0 cm/s for undulation pattern with phase angle of 0°at (a) 0.8T (b)T.

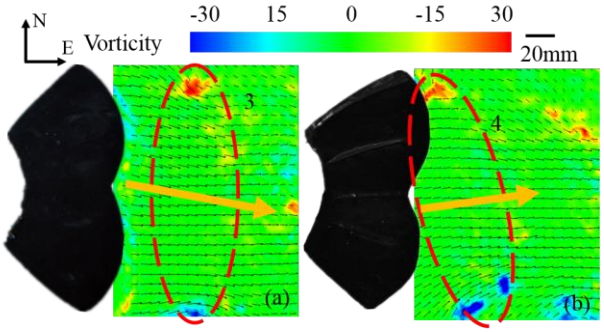

Figure 7. Instantaneous wake flow under U=10 cm/s for undulation pattern with phase angle of 0° at (a) 0.4T (b)0.8T. The diameter of vortex ring no. 3 and 4 were larger than that under U=0 cm/s.

At φ=90°, U=0cm/s, the morphology of the vortex rings were totally different than we have observed at φ=0° (U=0 cm/s and 10cm/s). The vortex rings were mainly shed from the upper lobe and R_0 and R were significantly smaller than those under φ=0°, U=0 cm/s, but α was greater than that of φ=0°, U=0 cm/s. For the entire flapping cycle, only one distinct vortex ring was shed at the instant of 0.2T. Comparing to vortex rings at φ=0°, U=0 cm/s, R_0, R and I both decreased significantly, however, α increased a little bit. Although the impulse of vortex ring no.5 on vertical direction was much smaller than vortex ring no. 1 and 2, the disorderly and unsystematic wake flow may contained a quantity of energy and provided a large portion of the lift force.

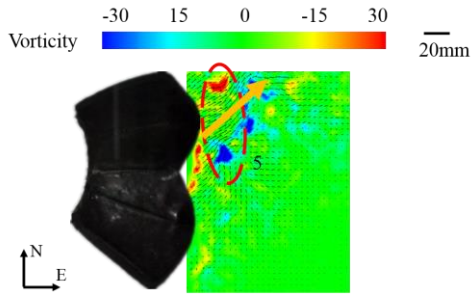

Figure 8. Instantaneous wake flow under U=0 cm/s for undulation pattern with phase angle of 90°at 0.2T. Only one vortex ring was produced by the caudal fin under this kinematic condition.

At U=0 cm/s, two distinct vortex rings appeared again during a complete cycle when phase φ increased to 270°. Different from the other three experimental groups, these two vortex rings were shed from the lower lobe at the time instant of 0.4T and 0.8T respectively (Fig. 9, vortex ring no. 6 and 7). The value of α demonstrated the vertical component of the impulse was mainly provided by the vortex ring no. 7 (α were -2.9° and 9.3° for vortex ring no. 6 and 7 respectively).

In general, as U increased, some parameters (R, and I) increased, some parameters (R_0, and α) decreased, some parameters (Φ, the number of vortex rings per flapping cycle and the vortex ring shedding site) changed little and the moment of shedding vortex rings was in advance. Although the increased flow speed enhanced the energy contained in vortex rings, the increased drag force counteracted the effect of the enhancement and led to a decreasing thrust force. Meanwhile, the decreasing jet flow angle resulted in the decrease on lift force. As φ varied, all the variables mentioned above may change. At φ=90°, U=0cm/s, the wake flow was disordered and we can only found one obvious and intact vortex ring during a flapping cycle. At other movement patterns, two vortex rings can be observed shedding behind the caudal fin per flapping period.

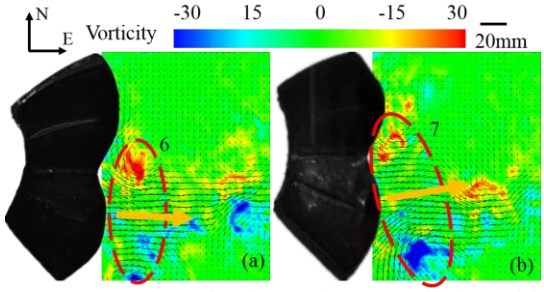

Figure 9. Instantaneous wake flow under U=0cm/s for undulation pattern with phase angle of 270°at (a) 0.4T (b)0.8T.

TABLE I. VORTEX PARAMETER

No	R_0 (mm)	R (mm)	Φ (deg)	α (deg)	Γ (mm^2s^{-1})	I (10^{-5}Ns)
1	20.73	45.30	89.27	2.76	15770	10170
2	14.12	31.26	84.51	32.21	11940	3670
3	9.80	71.39	89.27	-10.82	10910	17470
4	6.98	61.41	100.72	8.16	7230	8570
5	8.88	24.84	95.91	39.4	8150	1580
6	9.81	36.39	89.56	-2.58	8190	3410
7	11.18	40.47	104.31	9.32	11050	5690

IV. DISCUSSION AND CONCLUSIONS

Although there are some previous functional locomotor studies of biological caudal fin, the inability to manipulate and isolate key biomechanical parameters has hindered our understanding of caudal fin propulsion, for example, the hydrodynamic effect of caudal peduncle, the fin ray movement patterns and the swimming speed. The bio-robotic model described in this paper was designed to have capabilities of generating kinematics matching that of freely-swimming fishes, and the experimental apparatus allows for collecting quantitative hydrodynamic data, such as forces and instantaneous wake flow. The results show that the forces and wake flow are different when phase angle between peduncle and fin ray locomotion was changed. We summed up current experimental results and formulate several predictions as follows:

(I) Lift force decreases as flow speed increased as shown in Fig. 4(b). Although the increment of the oncoming flow enhanced the impulse of the vortex rings, the decreased jet angle counteract this effect, such as in Table I, the impulse of the vortex 3 is larger than that of the vortex 1, however, the former one possessed a smaller jet angle. We therefore hypothesize that fish may actively change their fin three-dimensional locomotor shapes to achieve considerable lift force at low swimming speed. At higher swimming speed, however, three-dimensional fin motions were not able to generate significant lift force. The decreased thrust force may

due to the increment of drag resulting from the oncoming flow increment and the net thrust force may increase as the impulse of the vortex ring was enhanced.

(II) Robotic fins with undulation motion can generate significantly larger lift forces. As we can see in Fig. 4(c) and (d), the lift and thrust force are in the same magnitude. The phase angle between fin ray and caudal peduncle motion is a key factor to determine the magnitude of the thrust and lift force. The magnitude of the average forces and the profile morphology of the instantaneous forces all varied with the phase angle changing.

(III) By cooperating the caudal fin ray and peduncle motion, fish may achieve the goal of wake controlling. The vortex ring shedding position, morphology parameters and impulse all shifted under the influence of the phase angle between caudal fin ray and peduncle (from Fig. 6 to Fig. 9, Table I). We therefore hypothesis that the caudal fin and the peduncle formed a "flexible vectoring propeller" and may be important for the three-dimensional maneuverability of fish swimming.

ACKNOWLEDGMENT

Many thanks to Zhu Qichao, Wang Yueping and Wang Zaijun for their help in implementing the experimental apparatus and programming motion of the robotic fin. And thanks to Israel for his help on polishing the article.

REFERENCES

[1] S. Alben, C. Witt, T. V. Baker, E. Anderson and G. V. Lauder, "Dynamics of freely swimming flexible foils," *Phys Fluids,* vol. 24, pp. 051901, May, 2012.

[2] J. Anderson, K. Streitlien, D. Barrett and M. Triantafyllou, "Oscillating foils of high propulsive efficiency," *J Fluid Mech,* vol. 360, pp. 41-72, 1998.

[3] L. Wen, T. M. Wang, G. H. Wu and J. H. Liang, "Hydrodynamic investigation of a self-propelled robotic fish based on a force-feedback control method," *Bioinspir Biomim,* vol. 7, pp. 036012, Sep, 2012.

[4] L. Wen, J. C. Weaver and G. V. Lauder, "Biomimetic shark skin: design, fabrication and hydrodynamic function," *J Exp Biol,* vol. 217, pp. 1656-66, May 15, 2014.

[5] T. M. Wang, L. Wen, G. H. Wu and J. H. Liang, "Quantitative thrust efficiency of a self-propulsive robotic fish: experimental method and hydrodynamic investigation," *Ieee-Asme T Mech,* vol. 18(3), pp. 1027-1038, 2013.

[6] T. M. Wang, Q. Shen, L. Wen and J. H. Liang, "On the thrust performance of an ionic polymer-metal composite actuated robotic fish: Modeling and experimental investigation," *Sci China Technol Sc,* vol. 55, pp. 3359-3369, Dec, 2012.

[7] G. V. Lauder, *Animal Locomotion*. Springer, 2010, pp. 3-15.

[8] W. C. Witt, L. Wen and G. V. Lauder, "Hydrodynamics of C-Start Escape Responses of Fish as Studied with Simple Physical Models," *Integr Comp Biol,* pp. icv016, 2015.

[9] G. V. Lauder, E. G. Drucker, J. C. Nauen and C. D. Wilga, "Experimental hydrodynamics and evolution: caudal fin locomotion in fishes," *Vertebrate Biomechanics and Evolution,* pp. 117-135, 2003.

[10] J. C. Nauen and G. V. Lauder, "Hydrodynamics of caudal fin locomotion by chub mackerel, Scomber japonicus (Scombridae)," *J Exp Biol,* vol. 205, pp. 1709-24, Jun, 2002.

[11] B. E. Flammang and G. V. Lauder, "Speed-dependent intrinsic caudal fin muscle recruitment during steady swimming in bluegill sunfish, Lepomis macrochirus," *J Exp Biol,* vol. 211, pp. 587-98, Feb, 2008.

[12] J. Oeffner and G. V. Lauder, "The hydrodynamic function of shark skin and two biomimetic applications," *J Exp Biol,* vol. 215, pp. 785-95, Mar 1, 2012.

[13] L. Wen and G. Lauder, "Understanding undulatory locomotion in fishes using an inertia-compensated flapping foil robotic device," *Bioinspir Biomim,* vol. 8, pp. 046013, Dec, 2013.

[14] M. S. Triantafyllou and G. S. Triantafyllou, "An efficient swimming machine," *Sci Am,* vol. 272, pp. 64-71, 1995.

[15] C. J. Esposito, J. L. Tangorra, B. E. Flammang and G. V. Lauder, "A robotic fish caudal fin: effects of stiffness and motor program on locomotor performance," *J Exp Biol,* vol. 215, pp. 56-67, Jan 1, 2012.

[16] O. M. Curet, N. A. Patankar, G. V. Lauder and M. A. MacIver, "Mechanical properties of a bio-inspired robotic knifefish with an undulatory propulsor," *Bioinspir Biomim,* vol. 6, pp. 026004, Jun, 2011.

[17] O. M. Curet, N. A. Patankar, G. V. Lauder and M. A. Maciver, "Aquatic manoeuvering with counter-propagating waves: a novel locomotive strategy," *J R Soc Interface,* vol. 8, pp. 1041-50, Jul 6, 2011.

[18] G. V. Lauder, "Fish locomotion: recent advances and new directions," *Annu Rev Mar Sci,* vol. 7, pp. 521-45, 2015.

[19] G. V. Lauder, J. Lim, R. Shelton, C. Witt, E. Anderson and J. L. Tangorra, "Robotic Models for Studying Undulatory Locomotion in Fishes," *Mar Technol Soc J,* vol. 45, pp. 41-55, Jul-Aug, 2011.

[20] B. E. Flammang and G. V. Lauder, "Caudal fin shape modulation and control during acceleration, braking and backing maneuvers in bluegill sunfish, Lepomis macrochirus," *J Exp Biol,* vol. 212, pp. 277-86, Jan, 2009.

[21] G. V. Lauder, B. Flammang and S. Alben, "Passive robotic models of propulsion by the bodies and caudal fins of fish," *Integr Comp Biol,* vol. 52, pp. 576-87, Nov, 2012.

[22] Q. C. Zhu, Y. J. Cai, R. Ding, Z. Y. Ren, T. M. Wang and L. Wen, "Bio-inspired flexible robotic caudal fin with three-dimensional locomotion," *Intelligent Control and Automation (WCICA)*, pp. 1881-1886, 2014.

[23] T. M. Wang, L. Wen, G. H. Wu and J. H. Liang, "Hybrid Undulatory Kinematics of a Robotic Mackerel (Scomber scombrus): Theoretical Modeling and Experimental Investiga-tion," *Sci China Technol Sc,* vol. 55(10), pp. 2941-2952, 2012.

[24] T. M. Wang, L. Wen, G. H. Wu and J. H. Liang, "Hydrodynamic investigation of a self-propulsive robotic fish based on a force-feedback control method.," *Bioinspir Biomim,* vol. 7, 2012.

[25] L. M. Milne-Thomson, *Theoretical aerodynamics*. Courier Dover Publications, 1966.